ASME Journal of Computing and Information Science in Engineering
Online journal at:
https://asmedigitalcollection.asme.org/computingengineering

Engineering-Guided Deep Learning of Melt-Pool Dynamics for Additive Manufacturing Quality Monitoring

Siqi Zhang
Industrial and Manufacturing Engineering,
The Pennsylvania State University,
University Park, PA 16801
e-mail: suz304@psu.edu

Hui Yang[1]
Industrial and Manufacturing Engineering,
The Pennsylvania State University,
University Park, PA 16801
e-mail: huy25@psu.edu

Zhuo Yang
System Integration Division,
National Institute of Standards and Technology,
Gaithersburg, MD 20899
e-mail: zhuo.yang@nist.gov

Yan Lu
System Integration Division,
National Institute of Standards and Technology,
Gaithersburg, MD 20899
e-mail: yan.lu@nist.gov

Additive manufacturing (AM) fabricates three-dimensional parts via layer-by-layer deposition and solidification of materials. Due to the complexity of this process, advanced sensing is increasingly employed to facilitate system visibility, leading to a large amount of high-dimensional and complex-structured data. While deep learning brings attractive characteristics for data-driven process monitoring and quality prediction, it is currently limited in the ability to assimilate engineering knowledge and offer model interpretability for understanding process–quality relationships. In addition, due to spatiotemporal correlations in AM, a melt-pool anomaly observed during fabrication is not always indicative of abnormal quality characteristics. There is a pressing need to go beyond pointwise analysis of melt pools and consider spatiotemporal effects for quality analysis. In this paper, we propose a novel feature learning framework guided by engineering knowledge for AM quality monitoring. First, engineering knowledge is integrated with deep learning to delineate various sources of process variations and extract melt-pool features that reflect quality-related relationships. Second, a 3D neighborhood model is designed to characterize spatiotemporal variations of melt pools based on their domain-informed features. The resulting 3D neighborhood profiles enable us to go beyond pointwise analysis of melt pools for capturing process–quality relationships. Finally, we built a regression model to predict internal density variations using 3D neighborhood profiles. Our experiments demonstrate that the proposed framework significantly outperforms traditional hand-crafted method and black-box learning in both the ability to provide quality-related features and predict internal density variations. [DOI: 10.1115/1.4066026]

Keywords: feature learning, engineering knowledge, process monitoring, quality control, additive manufacturing, melt pool, artificial intelligence, data-driven engineering, engineering informatics, machine learning for engineering applications

1 Introduction

Additive manufacturing (AM) entails the creation of three-dimensional parts by depositing and solidifying materials layer by layer. Given the complexity of this process, there is a growing reliance on advanced sensing for process monitoring and quality control. As a result, additive manufacturing processes generate a wide variety of high-dimensional and complex-structured data [1]. For example, as illustrated in Fig. 1(*a*), when powder materials are heated to their melting temperature by a high-energy laser, a melt pool is formed [2]. As the laser selectively fuses different points over space and time, co-axial images are continuously collected to monitor the evolving dynamics of melt pools, which are crucial for detecting process anomalies and optimizing control actions [3]. The post-build computed tomography (CT) data in Fig. 1(*b*) provides a high-resolution and three-dimensional representation of a fabricated part [4], which helps estimate defect levels in the fabricated part. This data availability offers an unprecedented opportunity to explore and understand process–quality interactions, but realizing its full potential for AM process monitoring and quality control hinges heavily on information-processing capabilities.

Handling imaging data is a general problem in additive manufacturing. Unlike time series and multi-channel signals, imaging data exhibit complex structures and lie in high-dimensional spaces. Traditional statistical quality control (SQC) methodologies often first extract a set of features from images and then build machine-learning models to establish process–quality relationships [5]. However, the efficacy of these approaches, along with their features depends heavily on model assumptions (i.e., linearity, stationary, scale invariance) that are made by human experts. On the other hand, deep learning methods focus on end-to-end learning, in which raw images are used as directed inputs to predict process conditions and quality levels as output neurons. Despite its superior

[1]Corresponding author.

Manuscript received December 1, 2023; final manuscript received July 2, 2024; published online August 6, 2024. Assoc. Editor: Linkan Bian.

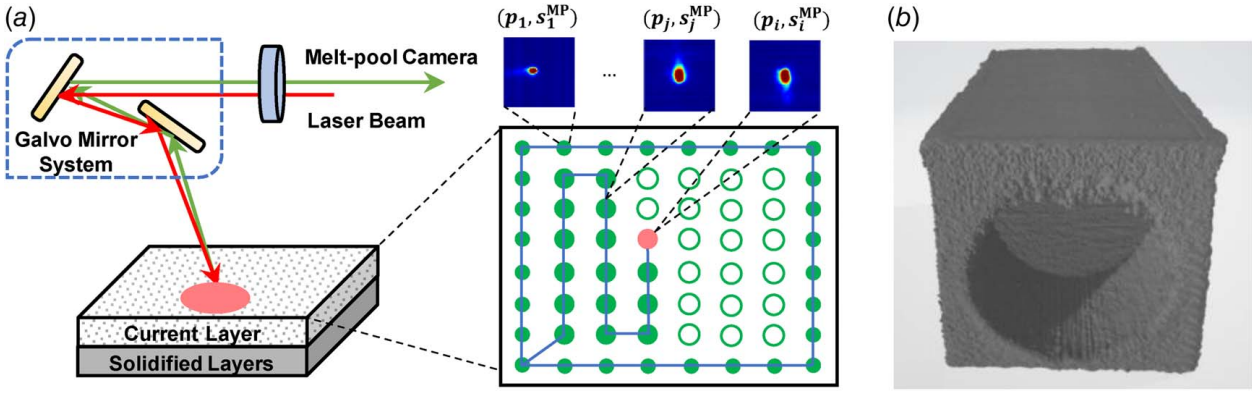

Fig. 1 Examples of AM sensing data: (*a*) melt-pool images collected in a laser-based AM and (*b*) CT scans of a fabricated part in a 3D voxelized structure

performance, this lack of model interpretability makes it challenging to explore and understand process–quality interactions, which is however crucial for AM quality control [6,7]. In addition, end-to-end learning needs a substantial amount of labeled data from post-build quality inspections to train the model, which is not readily available in real-world practices. An alternative way is to rely on deep neural networks to learn meaningful features from imaging data and then investigate complex relationships between process and quality in AM.

However, feature learning with deep neural networks is challenged by multiple variations inherent in an AM process. One critical signature in the process of laser-based additive manufacturing is the formation of melt pools. Because this is the onset of material solidification, melt-pool characteristics are highly associated with micro-structure and mechanical properties of fabricated parts. For example, matters ejected from the melt pool, also called spatter leads to stochastic lack-of-fusion flaws in laser powder bed fusion [8,9]. Besides, melt-pool characteristics are also sensitive to the change of process conditions, as shown in Fig. 2. Although these process differences tend to bring large variations to melt-pool morphological patterns, they are in-control operations and do not contribute to quality variability. This brings the challenge for traditional deep learning methods to learn quality-related features, as they focus on sparse representations of total variances rather than quality-related variance components. Hence, the assimilation of engineering knowledge into neural networks is essential to guide the deep learning process and facilitate the transformation of melt-pool images into features that are pertinent for AM quality characterization.

Another challenge resides in the spatiotemporal characterization of melt-pool variations for AM quality monitoring. As shown in Fig. 3, a part is created by selectively melting and solidifying powder materials using a laser over space and time. At each location, the formation of a melt pool is not independent, but influenced by its 3D neighboring region (i.e., either within the same layer or across adjacent layers). In addition, a laser not only melts powder to create melt pools, but also remelts a proportion of previously solidified materials belonging to 3D neighborhoods of previous melt pools. As such, a melt pool captured at one spatial location can only provide an incomplete picture of quality variations within the local area. In other words, due to spatiotemporal effects, a process anomaly (i.e., an abnormal melt pool) may not necessarily indicate abnormal quality characteristics in the corresponding locations of a fabricated part. It is imperative to go beyond pointwise analysis of melt pools and incorporate their spatiotemporal variations into the investigation of process–quality relationships [10].

In this paper, we propose a novel feature-learning framework guided by engineering knowledge to characterize melt-pool variations for AM quality monitoring. Specifically, we propose to

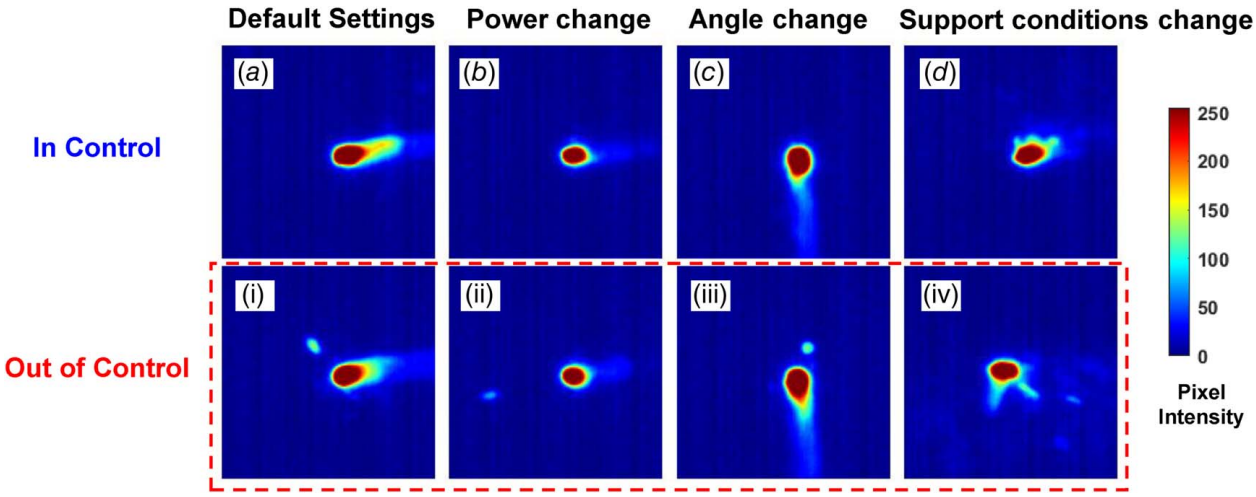

Fig. 2 Examples of process–quality interactions: illustration on how (*a*), (*i*) default settings with power =195 W, directional angle = + 180 deg, strong support; (*b*), (*ii*) power =100 W, directional angle = + 180 deg, strong support; (*c*), (*iii*) power =195 W, directional angle = + 90 deg, strong support; and (*d*), (*iv*) power =195 W, directional angle = +180 deg, weak support impact melt-pool characteristics. Note that melt pools in the first row are in-control, whereas those in the second row are out-of-control.

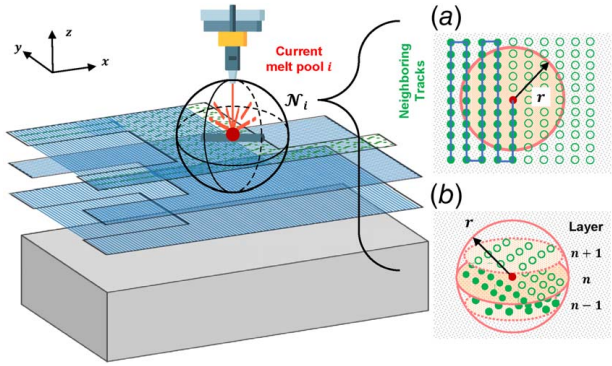

Fig. 3 3D spatiotemporal correlations in AM: (*a*) within the same layer and (*b*) across adjacent layers

integrate autoencoder structures with deep metric learning to build a domain-informed framework. The engineering knowledge is assimilated into deep metric learning to guide the integrated process and provide melt-pool features that can reflect quality-related relationships. Incorporating such knowledge will help learn quality-related relations between melt pools from different process conditions. Specifically, our contributions in this work are listed as follows:

(1) **Domain-informed feature learning**: In contrast to black-box learning, we propose to integrate engineering knowledge with deep learning for extracting domain-informed features of melt pools.
(2) **3D neighborhood modeling**: Then, we develop a 3D neighborhood model to capture spatiotemporal variations of melt pools. Such a representation enables the investigation of process–quality interactions that go beyond the pointwise level and account for spatiotemporal correlations in AM.
(3) **Process–quality interactions**: Finally, we build a predictive model to capture process–quality relationships and predict internal density variations via 3D neighborhood profiles for AM quality monitoring.

The remainder of this paper is organized as follows: Sec. 2 reviews related work. Section 3 presents the proposed framework including deep feature learning guided by engineering knowledge, 3D neighborhood modeling, and predictive modeling to predict internal density variations. Section 4 discusses experimental design and the results are provided in Sec. 5. Finally, Sec. 6 concludes this study.

2 Research Background

Feature learning is an essential task for extracting valuable information from sensing data to enable process monitoring and quality prediction in additive manufacturing. Over recent years, significant research efforts have been dedicated to analyzing images of build layers. For example, Yao et al. [11,12] proposed to extract the multi-fractal spectrum for the characterization of defect patterns within layerwise imaging. Liu et al. [13] developed an additive Gaussian process modeling framework to analyze within-layer and cross-layer variations for process monitoring. Liu and Yang also designed a novel approach to simulate the emission of photons for statistical estimation and modeling of the multimodal probability distribution function of melt pools [14]. Further, multiscale analyses have been conducted to extract complex and nonlinear patterns from layerwise images, including multi-resolution statistics from wavelet decomposition of layerwise images for in situ characterization of defect patterns [15] and superpixel attributes for the prediction of part density [16]. In addition to statistical approaches, efforts have been made to leverage deep learning for automated feature extraction and classification of different conditions. Caggiano et al. [17] built a deep convolutional neural network-based model to classify different defective conditions. In spite of these advancements, little has been done to shed insights on process phenomena pertinent to melt-pool dynamics during fabrication.

A melt pool is the result of laser-powder interactions on the particle level. Its dynamics not only reflect process stability, but also possess information related to the formation of microstructural defects. Real-time monitoring of melt-pool variations is thus critical to detect process and quality anomaly. In the state of the art, both co-axial and off-axial sensing systems have been integrated into AM machines to enable real-time monitoring of melt pool. The co-axial configuration aligns the camera with the laser injection path, resulting in more consistent locations of melt pools across different images. In contrast, an off-axial setup employs a stationary camera to capture the entire working area, regardless of the current location of a melt pool in the powder bed.

Upon the collection of melt-pool images, some researchers have focused on traditional SQC methodologies for AM process monitoring and quality control, which usually involves the following procedures: (1) image pre-processing, (2) feature extraction, and (3) statistical modeling. For example, Khanzadeh et al. [18] derived melt-pool characteristics via functional principal component analysis and then benchmarked several machine-learning algorithms to classify melt pools into different porosity groups. Scime and Beuth [19] extracted gradient information within melt-pool images to investigate how these signatures are correlated to keyholing porosity and balling instability in laser powder bed fusion. In addition, Zhang et al. [20] developed a multiscale basis function modeling framework to characterize 3D morphology of melt pools for manufacturing process monitoring. Yang et al. [21] performed a multilinear principal component analysis of melt-pool imaging tensor for extracting low-dimensional profiles, and then proposed a stochastic modeling framework to monitor spatiotemporal variations of melt-pool profiles. Guo et al. [22] developed a spatial–temporal conditional autoregressive model to characterize melt pools and then designed a two-level control chart for monitoring spatiotemporal variations of melt pools in a metal-based AM. However, most of the existing studies depend heavily on manual feature engineering, which is specific to model assumptions, datasets, and domain experts. As such, they tend to be limited in providing valuable insights into the manufacturing process that is beyond the scope of model, data, and expert opinions.

In addition, there are growing interests in deep learning with different architectures (e.g., convolutional neural networks (CNN), recurrent neural networks (RNN), and long short-term memory (LSTM)) for melt-pool characterization and monitoring. Among the relevant work, a lot of efforts have been made to build end-to-end learning between melt-pool images and different clustering groups related to process and quality. For example, Yang et al. [23] trained a CNN to classify melt pools into different size-related groups for anomaly detection. Kwon et al. [24] also trained a CNN to perform melt-pool classification but their study is more focused on classifying melt pools into different laser power settings. Further, there have been efforts to link melt-pool characteristics to porosity. Ho et al. [25] designed a residual-recurrent CNN with transfer learning to predict porosity from melt-pool images in a thin wall structure. Tian et al. [26] built an integrated framework with CNN for pyrometer data and LSTM for infrared camera data to classify porosity in a laser-based AM. Note that end-to-end learning often requires massive amount of labeled data to achieve high accuracy. However, obtaining such labels is time-consuming and expensive in real-world practices.

Alternatively, some researchers have focused on deep feature learning on melt-pool images for different AM tasks. For example, Fathizadan et al. [27] built a convolutional autoencoder to extract deep features from melt-pool images and then performed a hierarchical clustering algorithm for anomaly detection. Ko et al. [28] proposed to combine LSTM with a convolutional autoencoder to characterize spatiotemporal variations embedded in melt-pool imaging data for real-time monitoring of AM. Larsen and Hooper

[29] built a semi-supervised deep learning model with variational RNN for analyzing the imaging stream of melt pools and characterizing the AM dynamics. The dynamic signature from the proposed framework is then employed for anomaly detection and has proved to be useful for quantifying different levels of porosity.

In spite of great achievements discussed above, the following gaps in the literature are identified as follows:

(1) Although attempts have been made to leverage the power of deep learning for feature extraction, they are more concerned with black-box learning and do not enable the assimilation of engineering knowledge into neural network structures for managing various sources of process variations.
(2) Existing studies primarily rely on pointwise analysis of melt pools and do not account for the influence of spatiotemporal variations on part quality characteristics. Although Yang et al. [30,31] studied the fusion problem of 2D and 3D neighborhood modeling, their work focuses on physical properties (i.e., width, length, size of melt pools) and is limited in the ability to capture rich information hidden in melt-pool images. We posit the need to design a 3D neighborhood model with domain-informed features to capture spatiotemporal variations for quality characterization.
(3) Existing studies primarily focused on the characterization of melt-pool variations for porosity detection, but little has been done to investigate how melt-pool characteristics are correlated to internal density variations of a fabricated part.

3 Research Methodology

Figure 4 shows the proposed deep feature learning framework for AM quality monitoring. This framework differs from existing studies by enabling the integration of engineering knowledge to steer the feature learning process so as to provide melt-pool features closely tied to quality issues, as opposed to black-box features that account for various sources of process variability during fabrication. First, we design a neural network architecture with an autoencoder, deep metric learning, and a prediction module for domain-informed learning of melt-pool features. Specifically, engineering knowledge is fed into deep metric learning for guiding neural networks to project original images into the feature space that can reflect quality-related relationships. The prediction module is considered to classify melt pools into different conditions. Eventually, three modules are integrated together to guide neural network training and transform each melt-pool image into a set of domain-informed features. Second, we design a 3D neighborhood model to capture spatiotemporal variations of melt pools. A 3D neighborhood profile is then derived based on domain-informed features of melt pools belonging to the region. Such a design brings an attractive advantage to go beyond pointwise analysis of melt-pool features for investigating process–quality interactions. Finally, we build a predictive model of internal density variations using 3D neighborhood profiles for AM quality monitoring.

3.1 Domain-Informed Feature Learning.

In situ sensing of melt pools contains rich information related to ex situ part quality, but calls on domain-informed learning of melt-pool features to help reveal potential quality issues. Engineering knowledge such as how the melt pool relates to quality issues is crucial to guide deep neural networks and learn deep features that are salient to quality issues, as opposed to less informative features with in-control variations. As illustrated in Fig. 4, it is embodied by three components:

(1) a convolutional autoencoder for dimensionality reduction $f: \mathcal{X} \to \mathcal{Z}$, where $X_1, \ldots, X_T \in \mathcal{X}$ are melt-pool samples and $\mathbf{z} \in \mathcal{Z}$ is the latent representation of an input X.
(2) deep metric learning guided by engineering knowledge $g: \mathcal{Z} \to \mathcal{U}$, where $\mathbf{u} \in \mathcal{U}$ refers to the domain-informed feature vector.
(3) a prediction module $h: \mathcal{U} \to \mathcal{Y}$ for predicting the melt-pool condition, where $Y_1, \ldots, Y_T \in \mathcal{Y}$ are labeled conditions of melt pools by AM experts.

Note that the latent vector $\mathbf{z}$ has the same dimension as the domain-informed feature vector $\mathbf{u}$, but the former is the result without domain guidance. Our objective is to learn f, g, and h simultaneously, such that (1) a melt-pool sample X can be accurately reconstructed through latent representation $\mathbf{z}$; (2) the domain-informed feature vector of a melt-pool sample with a label k stays close to that of other samples with the same label in the latent space but be away from those with different labels; and (3) a classifier h can predict the melt-pool condition accurately.

3.1.1 Autoencoder for Dimensionality Reduction. The first module employs a convolutional autoencoder (CAE) but the objective here is to transform high-dimensional images into low-dimensional latent spaces. Formally, the CAE has three subcomponents: (1) an encoder to project an input $X \in \mathbb{R}^{I_1 \times I_2}$ into a latent representation $\mathbf{z} \in \mathbb{R}^{p \times 1}$, (2) a decoder to approximate the original input $\hat{X} \in \mathbb{R}^{I_1 \times I_2}$ through reverse transformation of the low-dimensional profile $\mathbf{z}$, and (3) a bottleneck between the encoder and decoder to store the latent representation $\mathbf{z}$. For a collection of melt-

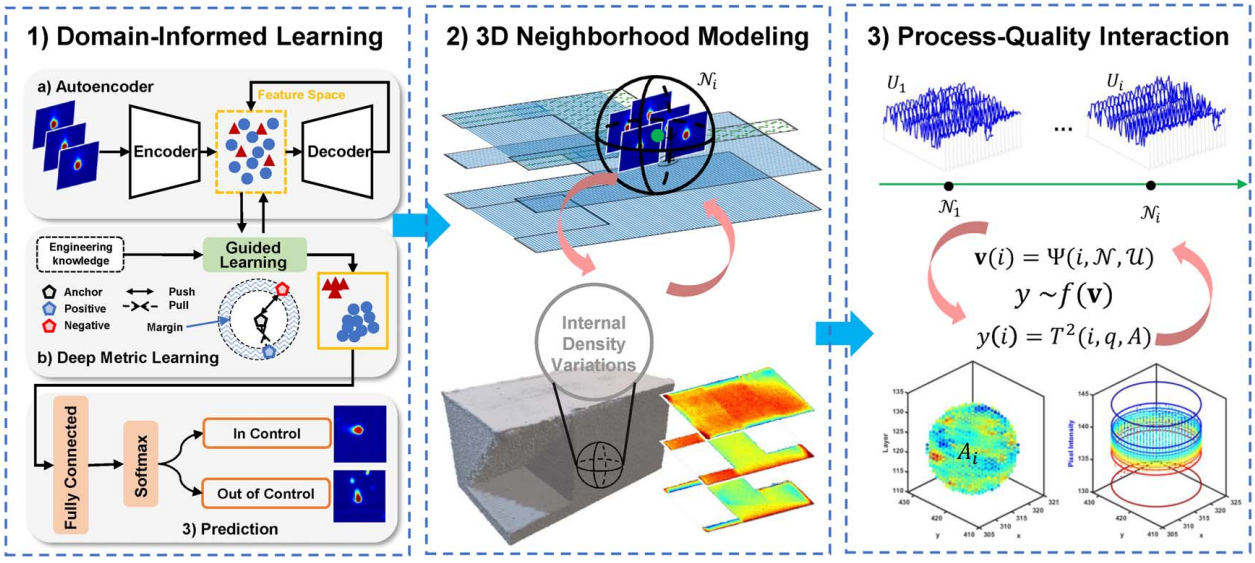

Fig. 4 Flow diagram of the proposed framework

pool images $X_1, \ldots, X_n$ collected at different time indices $i = 1, \ldots, n_T$, the training objective is to minimize the error between original data and its reconstruction

$$\mathcal{L}_{\text{MSE}}(X_i, \hat{X}_i) = \frac{1}{I_1 \times I_2} \|X_i - \hat{X}_i\|^2 \tag{1}$$

The encoder involves a stack of hidden layers with different functionality. For example, a convolutional layer is chosen to preserve spatial structures of melt-pool imaging data. A pooling layer immediately after the Conv2D is considered to retain salient features and help reduce the computational complexity of neural networks. In practice, these two types of layers are often combined as a block for effective learning of complex-structured images. In this investigation, such block is repeated three times in the encoder to make neural networks deep and disclose hidden information in melt-pool images. Finally, the resulting output is flattened and connected to a dense layer with the desired dimension for generating the latent representation $\mathbf{u}$ in the bottleneck. For the decoder, hidden layers are arranged in a symmetric way to those in the encoder for reconstructing original inputs.

3.1.2 Metric Learning With Engineering Knowledge. CAE helps extract a low-dimensional set of features (i.e., within the latent representation) from imaging data, but these features cannot reflect quality relations between images. Because material ejected from the melt pool, also called spatter, lead to defects in a laser-based powder bed fusion, we utilized this engineering knowledge to label melt-pool images into in-control and out-of-control groups. Surprisingly, the leading two features between in-control and out-of-control groups are mixed together in Fig. 5. In other words, an autoencoder alone, also black-box learning, is limited in providing salient features that are potentially related to quality characteristics. This calls upon the opening of the black box and assimilation of the above engineering knowledge to steer the deep feature learning process. Deep metric learning is an effective method for learning semantic relations between images via the representation of metric distances. However, few, if any previous studies have integrated engineering knowledge into deep metric learning of melt-pool dynamics for feature extraction in additive manufacturing.

Given a variety of melt-pool images related to different variations, our objective is to explicitly capture quality relations between melt-pool images via attract-repel operations and learn features that reflect this relation, as illustrated in Fig. 6. Given an anchor image X in the middle, because stochastic variations are less concerned with abnormal quality issues, these samples are positively related to the anchor and will be attracted in the feature space. In contrast, because the existence of spatter from the melt-pool image is related to quality concerns, these images on the right are negative samples and will be repelled by the anchor in the feature space. For a triplet of an anchor, positive and negative samples, we are interested in projecting them into a feature space such that

$$\phi(f(X), f(X^+)) \ll \phi(f(X), f(X^-)) \tag{2}$$

where $f(\cdot)$ is the encoder function and $\phi(\cdot)$ is the metric function to quantify the distances of features.

In particular, we formulate the triplet loss [32] to solve this problem, i.e.,

$$\mathcal{L}_{\text{DML}}(\mathbf{z}, \mathbf{z}^+, \mathbf{z}^-) = \max[\phi(\mathbf{z}, \mathbf{z}^+) - \phi(\mathbf{z}, \mathbf{z}^-) + \Delta, 0] \tag{3}$$

where $\mathbf{z} = f(X)$ is the feature vector of the anchor, $\phi(\mathbf{z}, \mathbf{z}^+)$ is the Euclidean distance between an anchor and the positive sample in the feature space. The triplet loss is formulated to mine three possible sets of triplets: (1) easy triplet: it occurs when the repel-attract relationship in Eq. (2) automatically satisfies and $\mathcal{L}_{\text{DML}} = 0$; (2) hard triplet: it occurs when $\phi(\mathbf{z}, \mathbf{z}^+) > \phi(\mathbf{z}, \mathbf{z}^-)$, indicating that we need to minimize the triplet loss of $\phi(\mathbf{z}, \mathbf{z}^+) - \phi(\mathbf{z}, \mathbf{z}^-) + \Delta$ so as to guarantee that the negative sample is not closer to the anchor than the positive sample and maintains a marginal distance of Δ; and (3) semi-hard triplet: it occurs when $\phi(\mathbf{z}, \mathbf{z}^+) + \Delta > \phi(\mathbf{z}, \mathbf{z}^-) > \phi(\mathbf{z}, \mathbf{z}^+)$ and the negative sample happens to appear in the marginal region. Overall, deep metric learning with engineering knowledge helps fine-tune deep features from the autoencoder so as to reflect quality relationships between melt-pool samples. As such, deep features of each melt-pool image $\mathbf{u}$ becomes domain-informed.

3.1.3 Prediction of Melt-Pool Conditions. The objective of this module is to predict whether a melt pool is out-of-control based on learned features. Specifically, the domain-informed feature vector $\mathbf{u}$ is fed into a fully connected layer with softmax activation h to classify the melt-pool condition in a probabilistic manner. For a K-class classification, there will be K neurons in the fully connected layer. Each neuron outputs a value $p_k(\mathbf{u})$ from 0 to 1 to describe how likely a melt-pool sample belongs to each of the class. As such, the sum of these outputs adds up to 1. The training objective of this module is to minimize the cross-entropy loss as follows:

$$\mathcal{L}_{\text{Entropy}}(y, \hat{y}) = -\sum_{k=1}^{K} y_k \log(\hat{y}_k) \tag{4}$$

where y_k and $\hat{y}_k$ are the ground truth and predicted probabilities of whether a melt pool belongs to a class k.

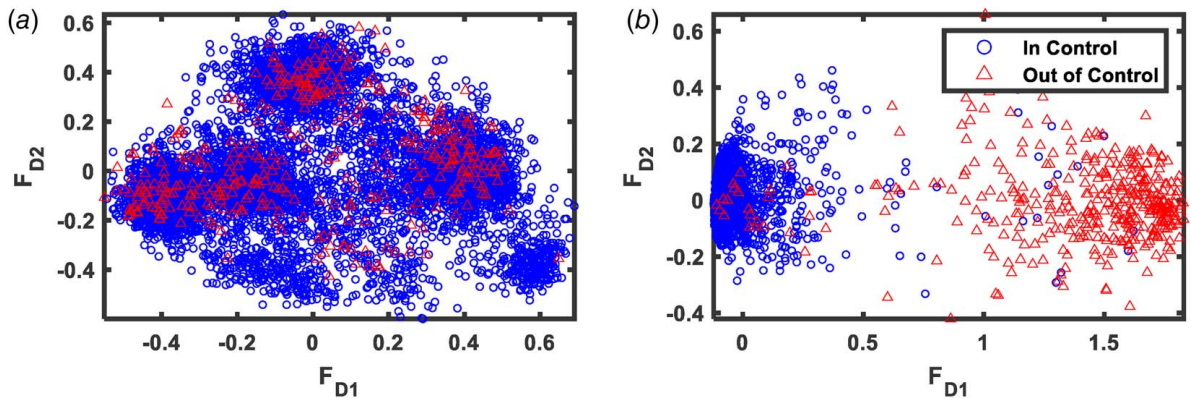

Fig. 5 Comparison of melt-pool features from (*a*) an autoencoder versus (*b*) the proposed domain-informed framework, where *x* and *y* axes refer to the first and second leading features, i.e., F_{D1} and F_{D1} respectively

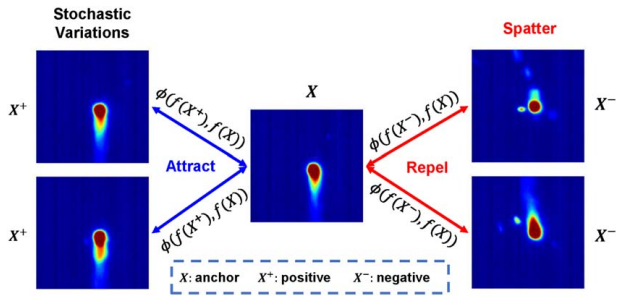

Fig. 6 Metric learning of stochastic and spatter-related variations

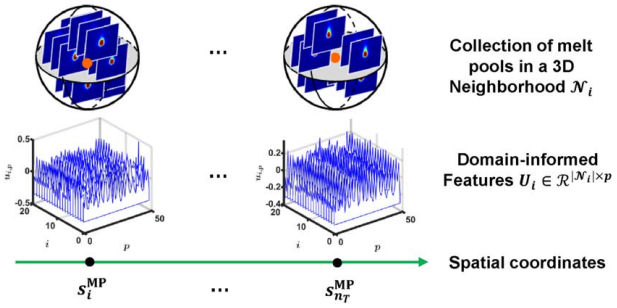

Fig. 7 Illustration of 3D neighborhood modeling of spatiotemporal variations

3.1.4 Network Training. Finally, the training objective of the domain-informed learning framework can be expressed as

$$\mathcal{L}_{total} = \frac{1}{n_T}\sum_{i=1}^{n_T}\{\gamma_1\mathcal{L}_{\text{MSE}}(X_i, \hat{X}_i) + \gamma_2\mathcal{L}_{\text{DML}}(\mathbf{z}_i, \mathbf{z}_i^+, \mathbf{z}_i^-) + \gamma_3\mathcal{L}_{\text{Entropy}}(y_i, \hat{y}_i)\} \tag{5}$$

where n_T is total number of melt-pool images and $\gamma_1, \gamma_2, \gamma_3$ denote the weights for different loss functions, respectively. The proposed framework offers the advantages of integrating AM knowledge into network training and learning domain-informed features for AM process characterization, as opposed to feature learning from a black-box perspective. After training, each melt-pool image is transformed into a set of domain-informed features. For a time-varying stream of melt-pool images $\mathcal{X} = [X_1, \ldots, X_{n_T}] \in I_1 \times I_2 \times n_T$, we have

Index	Spatial location	Melt-pool image	Domain-informed features
$i = 1$	$\mathbf{s}_1^{\text{MP}} \in \mathbb{R}^{1\times 3}$	$X_1 \in \mathbb{R}^{I_1\times I_2}$	$\mathbf{u}_1 = [u_{1,1}, \ldots, u_{1,p}] \in \mathbb{R}^{1\times p}$
$i = 2$	$\mathbf{s}_2^{\text{MP}} \in \mathbb{R}^{1\times 3}$	$X_2 \in \mathbb{R}^{I_1\times I_2}$	$\mathbf{u}_2 = [u_{2,1}, \ldots, u_{2,p}] \in \mathbb{R}^{1\times p}$
⋮	⋮	⋮	⋮
$i = n_T$	$\mathbf{s}_{n_T}^{\text{MP}} \in \mathbb{R}^{1\times 3}$	$X_{n_T} \in \mathbb{R}^{I_1\times I_2}$	$\mathbf{u}_{n_T} = [u_{n_T,1}, \ldots, u_{n_T,p}] \in \mathbb{R}^{1\times p}$

3.2 3D Neighborhood Modeling. Due to spatiotemporal correlations, an anomaly observed during the manufacturing process is not equivalent to abnormal quality characteristics. Thus, we propose a 3D neighborhood model to capture spatiotemporal variations of melt pools for AM process characterization. In particular, a 3D ball is considered to represent the neighborhood that is moving along the scan path to characterize process variations over space and time. As illustrated in Fig. 3, the 3D neighborhood of a melt pool i includes not only its neighboring tracks within the same layer but also neighboring layers, i.e.,

$$\mathcal{N}(i) = \{j \in \mathcal{S}^{\text{MP}} : \|\mathbf{s}_j^{\text{MP}} - \mathbf{s}_i^{\text{MP}}\|^2 < r^2\} \tag{6}$$

where $\mathcal{S}^{\text{MP}} = \{1, \ldots, n_T\}$ is the spatial domain of melt-pool locations, and r is the ball radius that controls the neighboring effect. For practical usages, the choice of the 3D neighborhoods depends on the design and process conditions of AM processes. If $\mathcal{N}(i)$ is too small, the 3D neighborhood only contains a current melt pool of its own and there will be no space–time correlations. On the contrary, if $\mathcal{N}(i)$ is too large, there will be an overflow of melt pools in the neighborhood and spatiotemporal relations tend to be undermined.

As shown in Fig. 7, the 3D neighborhood dynamically varies as the laser moves, selectively fusing different spatial points across the powder bed. At a specific spatial location $\mathbf{s}_i^{\text{MP}}$, all melt pools within the 3D neighborhood are collected to estimate spatiotemporal variations involved in the fabrication process. Let $|\cdot|$ is the cardinality of the neighborhood set. Then, there will be $|\mathcal{N}_i|$ melt pools associated with each neighborhood, leading to a set of domain-informed features $U_i \in \mathbb{R}^{|\mathcal{N}_i|\times p}$. Finally, 3D neighborhood variations can be expressed as

$$\mathbf{v}(i) = \Psi(i, \mathcal{N}_i, U_i) \tag{7}$$

where U_i is the set of domain-informed features within the 3D neighborhood of a melt pool i and Ψ is a function to map the set to a 3D neighborhood profile. In this investigation, we leverage individual variances of domain-informed features (i.e., the diagonal elements of its covariance matrix) to capture spatiotemporal variations in a 3D region. This leads to a 3D neighborhood profile $\mathbf{v} \in \mathbb{R}^{1\times p}$. The logic behind this is that when a melt pool exhibits abnormal variations that are different from its neighboring melt pools, its domain-informed features tend to have heterogeneous patterns. The use of individual variances is conducive to capturing such information.

3.3 Predicting Internal Density Variations Via 3D Neighborhood Profiles. Realizing the full potential of in situ melt pools for AM quality monitoring hinges on the establishment of its relationship with ex situ part quality. Because melt-pool images are complex-structured data, traditional deep learning applications often build end-to-end models, using melt-pool images as input and part quality characteristics as output to predict the quality of a fabricated part. These models typically involve a large number of parameters and complex structures for capturing process–quality interactions. In contrast, our proposed framework takes a different approach by first incorporating engineering knowledge into neural networks for feature learning and then characterizing spatiotemporal variations of melt pools for process characterization. Because complex-structured data have been transformed into a sparse set of salient features, a simpler model suffices to describe process–quality interactions.

This study focuses on a multivariate regression model for predicting internal density deviations from 3D neighborhood profiles. The ground truth about internal density deviations is established on the CT data. As opposed to traditional statistical analysis, we performed a stratified analysis to quantify density variations from the pixel intensity distribution of a 3D neighborhood. Specifically, the distribution of pixel intensity is stratified into several subgroups for extracting characteristics of local density variations. Each subgroup is associated with a distinct range of pixel intensities. As such, local variations will not be overlooked. Assume that A_i refers to the distribution of pixel intensity belonging to a 3D neighborhood $\mathcal{N}_i$ and $l = 1, \ldots, L$ refers to the stratified level. The lth level contour contains all points with a value that is greater than q_{l-1} but not more than q_l, where q_l is the lth level boundary value. Then, the discretized representation of the local density distribution $\zeta \in \mathbb{R}^{1\times L}$ is the percentage of pixel values falling into individual contours.

4 Experimental Design

The proposed framework is evaluated and validated with real-world experimental data (i.e., melt-pool imaging data [2], CT scans [4]) from a part fabricated in a metal-based AM system [33]. The fabrication of this part involves 250 layers and each layer is associated with about 5000 melt-pool images from the in situ sensing system. The laser parameters include 100 W and 900 mm/s scan speed for pre-contour scan, 195 W and 800 mm/s scan speed and 100 μm hatch spacing for infilling regions. The orientation of the laser scan rotates 90 degree every layer and alternatively starts the infilling scan from the top, left, bottom, and right sides of the part. Due to process uncertainty and variations, melt pools show a wide variety of different patterns, as illustrated in Fig. 2. On the other hand, post-build inspection is performed on a Zeiss Metrotom 800 machine with a voxel size of 11.95 μm $\times$ 11.95 μm $\times$ 11.95 μm. The yields CT data in the dimension of $774 \times 440 \times 440$, in which each CT voxel is a grayscale intensity value describing local density. Our objective is to evaluate the capability of the proposed domain-informed feature learning framework for capturing process–quality interactions.

First, we evaluated the performance of domain-informed learning for extracting melt-pool features. For network training, we used a total of 7024 melt-pool images, in which 80% and 20% are reserved for training and validating, respectively. The latent size in the bottleneck is set to be 50 to capture the most salient features while avoiding redundancy. We also adopted an equal weight for different tasks in the loss function. The number of epochs is set to be 100 unless an early stopping criterion is triggered. Once the model is trained, it can be used to generate deep features for new melt-pool imaging data. Then, we compared the proposed framework with two state-of-the-art methods for extracting melt-pool features

(1) **Hand-crafted Features**: Hand-crafted features are commonly employed to characterize melt pools. This investigation considered six such features, namely melt-pool length, width, area, ratio of length versus width, image intensity, and melt-pool intensity, which are estimated based on the literature [34,35].
(2) **Black-box learning**: The first module of the proposed framework is a convolutional autoencoder, the details of which are shown in Table 1. Because engineering knowledge is not incorporated into this module, training it alone can be understood as feature learning without domain guidance, i.e., black-box learning. To ensure consistency, the identical architecture of the first module is employed for our benchmark experiments.

Second, we performed a spatial autocorrelation analysis to study how a melt pool is correlated to nearby melt pools throughout the 3D space. This analysis is essential for quantifying the critical region of spatiotemporal correlations and determining the optimal size of 3D neighborhoods. In this investigation, we extended the idea of local indicator of spatial association [36] to measure the spatiotemporal autocorrelation of melt pools in a 3D neighborhood. For a melt pool i, its neighboring dependence (ND) can be expressed as follows:

$$\mathrm{ND}_i = \frac{(x_i - \bar{x})}{\sum_i (x_i - \bar{x})^2 / N} \sum_j w_{ij}(x_j - \bar{x}) \tag{8}$$

where x refers to a melt-pool property (e.g., melt-pool size), $w_{ij} \in \{0, 1\}$ is the spatial weight between a melt pool i and j depending on whether they are neighbors or not, and N is the total number of melt pools in the neighboring region. When ND_i is close to 0, there are few spatiotemporal autocorrelations between a melt pool and its neighbors. When ND_i is close to 1/–1, there is a strong positive/negative spatiotemporal autocorrelation. In the experiments, we first varied the radius of neighboring regions to be 100, 200, 300, 400, and 500 μm to investigate its impact on the neighboring dependence in the 2D space. Then, assuming the optimal 2D radius is also appropriate for 3D neighborhoods, the number of neighboring layers is varied to be $0, \pm1, \ldots, \pm4$ to analyze how they have an influence on the neighboring dependence in the 3D space. Note that the layer thickness is 20 μm. Our objective is to identify the optimal size of 3D neighborhoods for characterizing spatiotemporal variations of the given manufacturing process, thereby aiding in AM quality monitoring.

Third, we characterized density variations of each 3D neighborhood as follows: **(1) data registration between the in situ and ex situ domain**: Because the 3D neighborhood is defined in the in situ sensing domain, it is critical to translate it into the ex situ CT domain. For a set of reference points in the in situ domain, their correspondences in the ex situ domain can be estimated through affine transformation; **(2) Identify the neighboring region in CT data**: The 3D neighboring region is ball-shaped, whereas CT data are consisted of cube-shaped voxels. In order to extract it from voxelized CT data, we first identified its inscribed cube and then generated a binarized mask to separate the neighboring region from the remaining proportion; **(3) Stratified analysis of internal density variations**: As detailed in Sec. 3.3, we stratified the pixel values of the neighboring region into different contours. This is similar to estimating probability density function from data in a histogram. Then, local density deviations ζ of each neighborhood are the percentages of pixels residing within each contour; **(4) Estimate the response variable of predictive modeling**: This step aims to transform the vector-form ζ into the response variable in a scalar form. Accounting for the variability of pixels residing in different contours, the Hotelling T^2 statistic is considered, i.e., $\lambda_{T^2} =$

Table 1 Detailed structure of the convolutional autoencoder

Structure	Layer	Filter	Stride	Activation	Output
Encoder	Conv2D	16	1	ReLu	16 @ 120 × 120
	MaxPooling2D	—	—	—	16 @ 60 × 60
	Conv2D	8	1	ReLu	8 @ 60 × 60
	MaxPooling2D	—	—	—	8 @ 30 × 30
	Conv2D	4	1	ReLu	4 @ 30 × 30
	MaxPooling2D	—	—	—	4 @ 15 × 15
	Flatten	—	—	—	900
	Dense	—	—	—	50
Bottleneck	Normalize	—	—	—	50
Decoder	Dense	—	—	—	900
	Reshape	—	—	—	4 @ 15 × 15
	Conv2DTranspose	4	2	ReLu	4 @ 30 × 30
	Conv2DTranspose	8	2	ReLu	8 @ 60 × 60
	Conv2DTranspose	16	2	ReLu	16 @ 120 × 120
	Conv2DTranspose	1	1	Sigmoid	1 @ 120 × 120

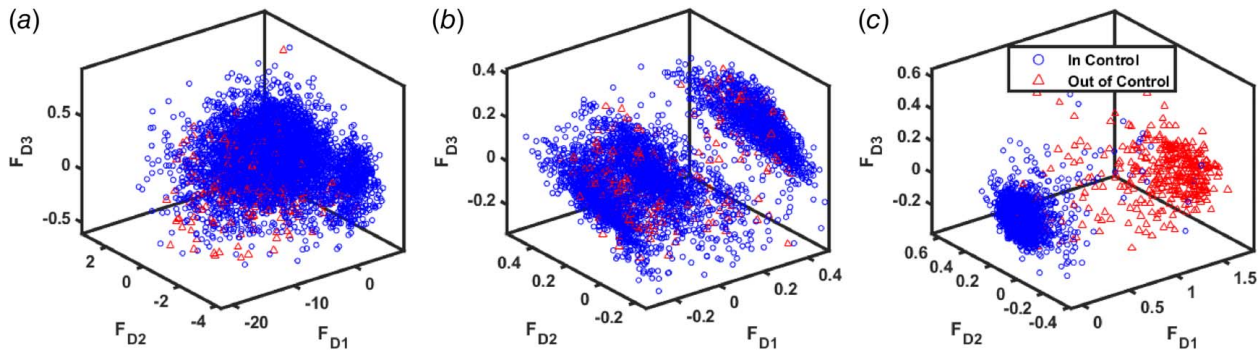

Fig. 8 3D visualization of (*a*) hand-crafted, (*b*) black-box, and (*c*) domain-informed features

$(\zeta - \bar{\zeta})\Sigma_{\zeta}^{-1}(\zeta - \bar{\zeta})^T$ where $\bar{\zeta}$ is the in-control mean and Σ_{ζ} is the in-control covariance matrix. The in-control 3D neighborhood is assumed to have a low percentage of spatters (i.e., <5%).

Finally, we built a predictive model to capture process–quality relationships and predict internal density deviations via 3D neighborhood profiles. The adjusted R^2 is then employed to evaluate the model performance. A higher value indicates a better explainability of internal density deviations using melt-pool features.

5 Experimental Results

5.1 Domain-Informed Feature Learning. We first demonstrated the effectiveness of the proposed domain-informed framework in extract salient features of melt pools. Figure 8 shows the comparison of hand-crafted, black-box, and domain-informed features in 3D scatter plots. Here, each point represents a melt pool from either an in-control or out-of-control group. With respect to hand-crafted features, it is evident in Fig. 8(*a*) that the majority of out-of-control melt pools tend to mix together with in-control melt pools and there is no significant boundary between the two groups. In other words, hand-crafted features are limited in the ability to distinguish between in-control and out-of-control melt pools. Second, as shown in Fig. 8(*b*) for black-box features, although melt pools tend to be more scattered around the 3D space, this is not related to out-of-control variations but the change of process conditions (e.g., laser power, scan direction) that are common during the manufacturing process. Moreover, a similar pattern of mix-ups can be observed between in-control and out-of-control melt pools at a specific process condition (i.e., a cluster in the figure). In total, black-box features are significant to in-control process uncertainties, but are less concerned with out-of-control variations related to quality characteristics. On the contrary, in-control melt pools are significantly separated from these out-of-control ones in Fig. 8(*c*), regardless of the change in manufacturing process conditions. This demonstrates the superiority of domain-informed learning framework over other methods in extracting salient features embedded in melt-pool images for AM process and quality characterization.

5.2 3D Neighborhood Modeling. 3D neighborhood modeling enables the characterization of melt-pool variations over both space and time, but one central question is how to determine the optimal size of 3D neighborhoods for a given AM process. As detailed in Sec. 4, we conducted a spatial autocorrelation analysis to investigate how ND varies with the radius of 2D neighborhood as well as the number of neighboring layers when expanding the 2D ball to a 3D sphere, thereby helping answer the question. The experiments were performed on 3148 neighborhoods centering on five different layers using melt-pool size as the primary property in Eq. (8).

Figure 9(*a*) shows the box plots of neighboring dependence when the 2D radius r is varied from 100 μm to 500 μm, in which dots refer to the mean, the boundary of the lower and upper whiskers refers to the minimum and maximum of estimated ND excluding outliers (i.e., plus signs), respectively. When r equals to 100 μm, ND ranges from -1 to 0 with a mean of -0.42, indicating that there are strong negative autocorrelations through the 2D spatial space. However, as the neighboring radius r increases, the spread of the distribution reduces significantly along with the mean closely approaching to 0. When r exceeds 300, there are only few variations in ND and the mean remains relatively stable. The value of $r = 300\,\mu$m is sufficient enough to capture spatiotemporal variations of the given AM process. Further, several outliers can be observed in the box plots, indicating that these neighboring regions are different than the majority of other neighborhoods in terms of

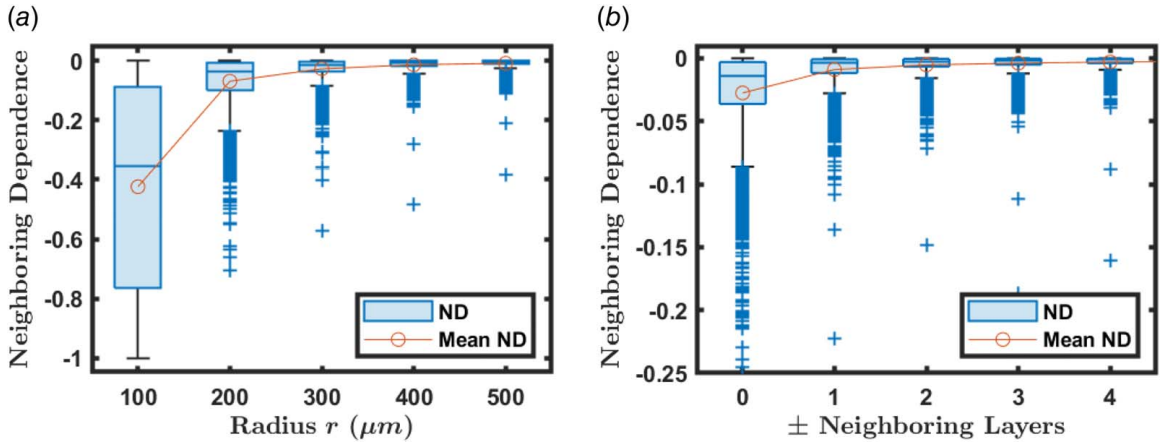

Fig. 9 The variations of ND with respect to (*a*) radius *r* and (*b*) number of ± neighboring layers

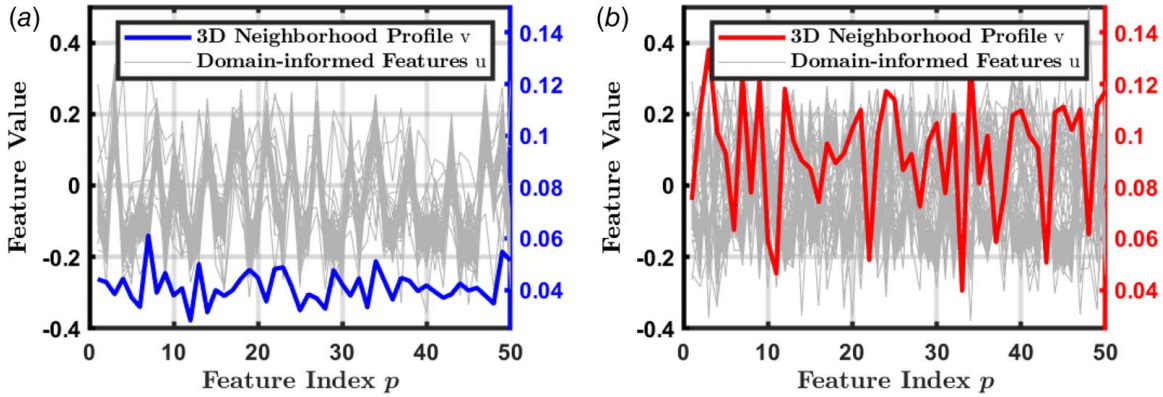

Fig. 10 3D neighborhood profiles of (*a*) an in-control versus (*b*) an out-of-control region. Note that bold curves refer to 3D neighborhood profiles, whereas the others refer to domain-informed features of neighboring melt pools

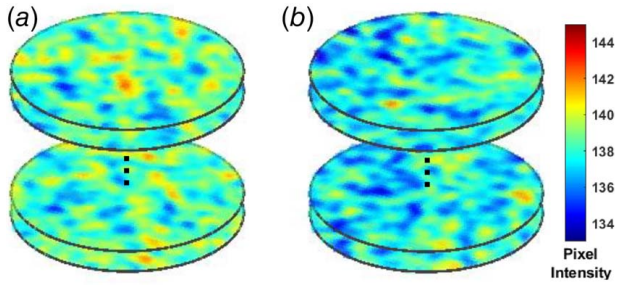

Fig. 11 Registered CT neighborhood of (*a*) in-control region with $\lambda_{T^2} = 12.55$ and (*b*) out-of-control region with $\lambda_{T^2} = 952.87$

spatiotemporal effects. Figure 9(*b*) shows the variations of neighboring dependence when different numbers of neighboring layers are included in the 3D sphere with a radius of $r = 300\,\mu$m. Neighboring melt pools within the same layer (i.e., ±neighboring layers = 0) report the lowest ND with a central melt pool. When more melt pools from nearby layers are included in the 3D neighborhood, the mean ND starts to increase. A relatively stable pattern can be observed when the number of ± neighboring layers is greater than 2. Hence, for the given dataset and AM process, a 3D neighborhood with a radius of 300 μm and ±2 neighboring layers is preferable to capture spatiotemporal variations of melt pools over the 3D space.

Then, a 3D neighborhood profile $\mathbf{v}$ can be estimated from domain-informed features of neighboring melt pools and their feature variances. As shown in Fig. 10, melt-pool features $\mathbf{u} = [u_1, \ldots, u_p]$ from an in-control region tend to have consistent patterns along the feature index p, whereas those from an out-of-control region tend to have large fluctuations along the feature index p. As a result, 3D neighborhood profile $\mathbf{v}$ of the out-of-control region (i.e., the bold curve in Fig. 10(*b*)) also has larger values than that of the other (i.e., the bold curve in Fig. 10(*a*)). These results demonstrate that 3D neighborhood profiles encompass valuable information pertaining to in-control and out-of-control regions, which is conducive to analyzing process–quality interactions in the following subsections.

5.3 Predictive Modeling of Computed Tomography Density Variations. Following detailed procedures in Sec. 4, we can estimate the value of the Hotelling T^2 statistic λ_{T^2} for characterization density variations in each 3D neighborhood. Figure 11 shows the comparison of two registered CT neighborhoods with different λ_{T^2}. As the value of λ_{T^2} increases, the CT neighborhood tends to have more local variations in low-pixel intensities. This demonstrates that λ_{T^2} is effective in capturing internal density variations from CT data. It is further utilized as the response variable of the predictive model to investigate the process–quality interaction. Next, we develop regression models to predict density variations using 3D neighborhood representations of melt-pool variations. The predictors are 50 features of 3D neighborhood profiles $\mathbf{v}$, as illustrated in Fig. 10. The response variable is the log-transformation of λ_{T^2} so as to stabilize variances for regression models. There are 3148 3D neighborhoods, the center of which are distributed in five different layers.

Figure 12 shows the comparison of predictive models using 3D neighborhood profiles of hand-crafted, black-box, and domain-

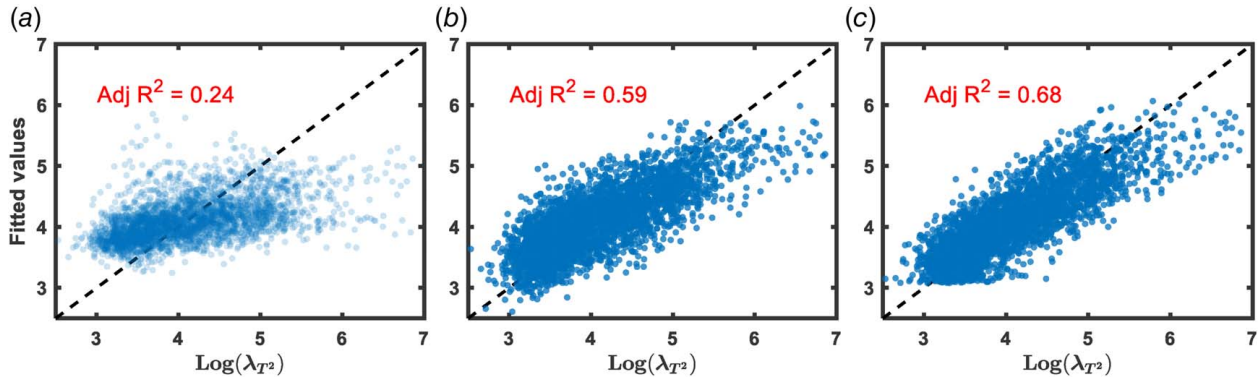

Fig. 12 (*a*) Performance comparison of regression models with (*a*) hand-crafted, (*b*) black-box, and (*c*) domain-informed features for predicting density variations

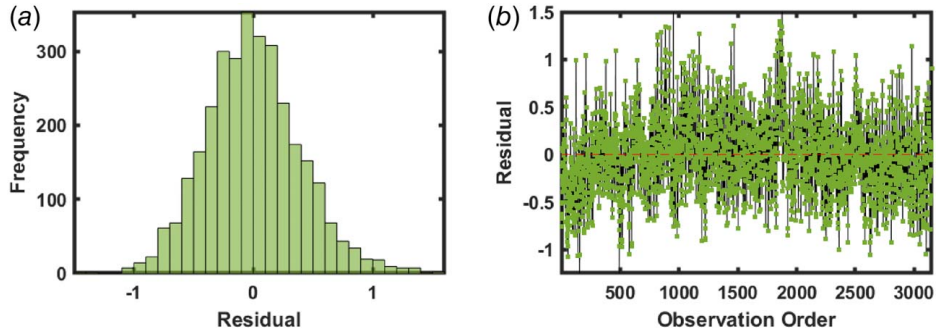

Fig. 13 Residual analysis of the predictive model with domain-informed features: (*a*) histogram of residuals and (*b*) plot of observed order versus residual

informed features as the predictors, respectively. Notably, the third model yields the best performance with an adjusted R^2 of 0.68. In other words, 68% of internal density variations can be explained by 3D neighborhood fusion of domain-informed features. This is primarily due to the superior performance of the proposed framework in exploiting domain knowledge into feature learning. In contrast, 3D neighborhood fusion of six shape-related features only achieves an adjusted R^2 of 0.24 in quantifying internal density variations, indicating these features tend to be limited to be employed for AM quality control. The performance measure of the regression model using black-box features is between the first and third models. Overall, these results demonstrate that the proposed domain-informed feature learning framework and 3D neighborhood modeling provide significant features for capturing process–quality interactions. Finally, the results of model diagnosis are provided in Fig. 13, in which the normal assumption of residuals is valid and no systematic pattern can be observed.

6 Conclusions

Modern manufacturing industries are investing in advanced sensing and information techniques, leading to data-rich environments in AM systems. This offers a great opportunity to investigate and understand process–quality relationships, which is crucial for AM quality control. Although deep learning has the potential to improve the autonomous and intelligent level of information extraction in AM systems, relevant studies reported in the literature often rely on black-box feature learning, while ignoring the fact that AM encompasses various sources of process variations (e.g., laser power, support conditions). As a result, learned features are primarily associated with in-control process variations, rather than out-of-control process variations that closely relate to quality characteristics. Furthermore, due to spatiotemporal effects, a process anomaly is not equivalent to abnormal quality characteristics in corresponding locations of a fabricated part. However, existing work primarily focuses on pointwise analysis of melt pools and tends to overlook spatiotemporal variations in part quality characteristics.

This paper presents a novel feature learning framework guided by engineering knowledge for AM quality monitoring. First, we design a neural network architecture with deep metric learning to delineate different sources of process variations and steer the feature learning process. Next, we design a 3D neighborhood model to capture spatiotemporal variations of melt pools. This allows us to explore process–quality relationships that account for spatiotemporal variations of the manufacturing process. Finally, we built a multivariate regression model to predict internal density variations with individual features of 3D neighborhood profiles as predictors.

The proposed framework is then evaluated and validated with real-world AM data. Benchmark experiments demonstrated that domain-informed learning helps extract melt-pool features related to out-of-control variations, as opposed to in-control uncertainties due to the change of process conditions. This is conducive to analyzing process–quality interaction in AM. Furthermore, experimental results showed that 3D neighborhood modeling effectively characterizes spatiotemporal dynamics of an AM process and provides salient features to predict internal density variations for AM quality monitoring.

This work improves AM imaging analysis through engineering-guided deep learning and 3D neighborhood modeling. The proposed framework makes an innovative attempt in integrating engineering knowledge into deep metric learning of melt-pool dynamics for feature extraction, but this model is limited in its ability to make predictions on future melt pools. In future work, it is worthwhile investigating real-time prediction of melt-pool dynamics. Deep learning methods such as generative adversarial networks can be explored to generate realistic melt-pool images based on process conditions and historical data.

Acknowledgment

This work was supported by the National Institute of Standards and Technology (NIST) under the cooperative agreement 70NANB19H127. The authors would like to thank NIST for supporting this research and acknowledge NIST colleagues Dr. Shawn Feng, Dr. Paul Witherell, and Dr. Albert Jones for providing comments and feedback to improve the quality of this work.

Conflict of Interest

There are no conflicts of interest.

Data Availability Statement

The datasets generated and supporting the findings of this article are obtainable from the corresponding author upon reasonable request.

Disclaimer

Certain commercial systems are identified in this paper. Such identification does not imply recommendation or endorsement by NIST; nor does it imply that the products identified are necessarily the best available for the purpose. Further, any opinions, findings, conclusions, or recommendations expressed in this material are those of the authors and do not necessarily reflect the views of NIST or any other supporting US government or corporate organizations.

References

[1] Yang, H., Kumara, S., Bukkapatnam, S. T., and Tsung, F., 2019, "The Internet of Things for Smart Manufacturing: A Review," IISE Trans., **51**(11), pp. 1190–1216.

[2] Lane, B., and Yeung, H., 2020, "Process Monitoring Dataset From the Additive Manufacturing Metrology Testbed (AMMT): Overhang Part X4," J. Res. Natl. Inst. Stand. Technol., **125**, pp. 1–18.
[3] Yao, B., and Yang, H., 2018, "Constrained Markov Decision Process Modeling for Sequential Optimization of Additive Manufacturing Build Quality," IEEE Access, **6**, pp. 54786–54794.
[4] Praniewicz, M., Lane, B., Kim, F., and Saldana, C., 2020, "X-ray Computed Tomography Data of Additive Manufacturing Metrology Testbed (AMMT) Parts: "Overhang Part X4," J. Res. Natl. Inst. Stand. Technol., **125**, pp. 1–9.
[5] Yang, H., Rao, P., Simpson, T., Lu, Y., Witherell, P., Nassar, A. R., Reutzel, E., and Kumara, S., 2020, "Six-Sigma Quality Management of Additive Manufacturing," Proc. IEEE, **109**(4), pp. 347–376.
[6] Yazdi, R. M., Imani, F., and Yang, H., 2020, "A Hybrid Deep Learning Model of Process-Build Interactions in Additive Manufacturing," J. Manuf. Syst., **57**, pp. 460–468.
[7] Imani, F., Chen, R., Diewald, E., Reutzel, E., and Yang, H., 2019, "Deep Learning of Variant Geometry in Layerwise Imaging Profiles for Additive Manufacturing Quality Control," ASME J. Manuf. Sci. Eng., **141**(11), p. 111001.
[8] Yin, J., Wang, D., Yang, L., Wei, H., Dong, P., Ke, L., Wang, G., Zhu, H., and Zeng, X., 2020, "Correlation Between Forming Quality and Spatter Dynamics in Laser Powder Bed Fusion," Addit. Manuf., **31**, p. 100958.
[9] Snow, Z., Scime, L., Ziabari, A., Fisher, B., and Paquit, V., 2023, "Observation of Spatter-Induced Stochastic Lack-of-Fusion in Laser Powder Bed Fusion Using In Situ Process Monitoring," Addit. Manuf., **61**, p. 103298.
[10] Chen, Y., and Yang, H., 2015, "Sparse Modeling and Recursive Prediction of Space–Time Dynamics in Stochastic Sensor Networks," IEEE Trans. Autom. Sci. Eng., **13**(1), pp. 215–226.
[11] Yao, B., Imani, F., Sakpal, A. S., Reutzel, E. W., and Yang, H., 2018, "Multifractal Analysis of Image Profiles for the Characterization and Detection of Defects in Additive Manufacturing," ASME J. Manuf. Sci. Eng., **140**(3), p. 031014.
[12] Imani, F., Yao, B., Chen, R., Rao, P., and Yang, H., 2019, "Joint Multifractal and Lacunarity Analysis of Image Profiles for Manufacturing Quality Control," ASME J. Manuf. Sci. Eng., **141**(4), p. 044501.
[13] Liu, R., Vogt, B. D., and Yang, H., 2021, "Gaussian Process Monitoring of Layerwise-Dependent Imaging Data," IEEE Rob. Autom. Lett., **6**(4), pp. 8029–8036.
[14] Liu, R., and Yang, H., 2023, "Multimodal Probabilistic Modeling of Melt Pool Geometry Variations in Additive Manufacturing," Addit. Manuf., **61**, p. 103375.
[15] Yang, H., Reijonen, J., and Revuelta, A., 2023, "Multiresolution Quality Inspection of Layerwise Builds for Metal 3D Printer and Scanner," ASME J. Manuf. Sci. Eng., **145**(10), p. 101004.
[16] Lu, Q., Grasso, M., Le, T.-P., and Seita, M., 2022, "Predicting Build Density in L-PBF Through In-Situ Analysis of Surface Topography Using Powder Bed Scanner Technology," Addit. Manuf., **51**, p. 102626.
[17] Caggiano, A., Zhang, J., Alfieri, V., Caiazzo, F., Gao, R., and Teti, R., 2019, "Machine Learning-Based Image Processing for On-Line Defect Recognition in Additive Manufacturing," CIRP Ann., **68**(1), pp. 451–454.
[18] Khanzadeh, M., Chowdhury, S., Marufuzzaman, M., Tschopp, M. A., and Bian, L., 2018, "Porosity Prediction: Supervised-Learning of Thermal History for Direct Laser Deposition," J. Manuf. Syst., **47**, pp. 69–82.
[19] Scime, L., and Beuth, J., 2019, "Using Machine Learning to Identify In-Situ Melt Pool Signatures Indicative of Flaw Formation in a Laser Powder Bed Fusion Additive Manufacturing Process," Addit. Manuf., **25**, pp. 151–165.
[20] Zhang, S., Lu, Y., and Yang, H., 2024, "Multiscale Basis Modeling of 3D Melt-Pool Morphological Variations for Manufacturing Process Monitoring," Int. J. Adv. Manuf. Technol., pp. 1–12.
[21] Yang, H., Zhang, S., Lu, Y., Witherell, P., and Kumara, S., 2022, "Spatiotemporal Monitoring of Melt-Pool Variations in Metal-Based Additive Manufacturing," IEEE Rob. Autom. Lett., **7**(3), pp. 8249–8256.
[22] Guo, S., Guo, W. G., and Bain, L., 2020, "Hierarchical Spatial-Temporal Modeling and Monitoring of Melt Pool Evolution in Laser-Based Additive Manufacturing," IISE Trans., **52**(9), pp. 977–997.
[23] Yang, Z., Lu, Y., Yeung, H., and Krishnamurty, S., 2019, "Investigation of Deep Learning for Real-Time Melt Pool Classification in Additive Manufacturing," 2019 IEEE 15th International Conference on Automation Science and Engineering (CASE), Vancouver, BC, Canada, Aug. 22–26, IEEE, pp. 640–647.
[24] Kwon, O., Kim, H. G., Ham, M. J., Kim, W., Kim, G.-H., Cho, J.-H., Kim, N. I., and Kim, K., 2020, "A Deep Neural Network for Classification of Melt-Pool Images in Metal Additive Manufacturing," J. Intell. Manuf., **31**(2), pp. 375–386.
[25] Ho, S., Zhang, W., Young, W., Buchholz, M., Al Jufout, S., Dajani, K., Bian, L., and Mozumdar, M., 2021, "DLAM: Deep Learning Based Real-Time Porosity Prediction for Additive Manufacturing Using Thermal Images of the Melt Pool," IEEE Access, **9**, pp. 115100–115114.
[26] Tian, Q., Guo, S., Melder, E., Bian, L., and Guo, W. G., 2021, "Deep Learning-Based Data Fusion Method for In Situ Porosity Detection in Laser-Based Additive Manufacturing," ASME J. Manuf. Sci. Eng., **143**(4), p. 041011.
[27] Fathizadan, S., Ju, F., and Lu, Y., 2021, "Deep Representation Learning for Process Variation Management in Laser Powder Bed Fusion," Addit. Manuf., **42**, p. 101961.
[28] Ko, H., Kim, J., Lu, Y., Shin, D., Yang, Z., and Oh, Y., 2022, "Spatial-Temporal Modeling Using Deep Learning for Real-Time Monitoring of Additive Manufacturing," International Design Engineering Technical Conferences and Computers and Information in Engineering Conference, St. Louis, Missouri, USA, August 14–17, 2022.
[29] Larsen, S., and Hooper, P. A., 2022, "Deep Semi-Supervised Learning of Dynamics for Anomaly Detection in Laser Powder Bed Fusion," J. Intell. Manuf., **33**(2), pp. 457–471.
[30] Yang, Z., Lu, Y., Yeung, H., and Krishnamurty, S., 2020, "From Scan Strategy to Melt Pool Prediction: A Neighboring-Effect Modeling Method," ASME J. Comput. Inf. Sci. Eng., **20**(5), p. 051001.
[31] Yang, Z., Lu, Y., Yeung, H., and Kirshnamurty, S., 2020, "3D Build Melt Pool Predictive Modeling for Powder Bed Fusion Additive Manufacturing," 2020 International Design Engineering Technical Conferences and Computers and Information in Engineering Conference, Virtual, Online, Aug.17–19.
[32] Schroff, F., Kalenichenko, D., and Philbin, J., 2015, "FaceNet: A Unified Embedding for Face Recognition and Clustering," the IEEE Conference on Computer Vision and Pattern Recognition (CVPR), Boston, MA, June 7–12, pp. 815–823.
[33] Lane, B., Mekhontsev, S., Grantham, S., Vlasea, M., Whiting, J., Yeung, H., Fox, J., Zarobila, C., Neira, J., McGlauflin, M., and Hanssen, L., 2016, "Design, Developments, and Results From the NIST Additive Manufacturing Metrology Testbed (AMMT)," 2016 International Solid Freeform Fabrication Symposium, The University of Texas in Austin, Aug. 8–10.
[34] Lane, B., Yeung, H., and Yang, Z., 2022, "Statistical and Spatio-Temporal Data Features in Melt Pool Monitoring of Additive Manufacturing," 2022 IISE Annual Conference, Seattle, WA, USA, May 21–24, pp. 1–6.
[35] Yang, Z., Adnan, M., Lu, Y., Cheng, F.-T., Yang, H.-C., Perisic, M., and Ndiaye, Y., 2022, "Investigating Statistical Correlation Between Multi-modality In-Situ Monitoring Data for Powder Bed Fusion Additive Manufacturing," 2022 IEEE 18th International Conference on Automation Science and Engineering (CASE), Mexico City, Mexico, Aug. 20–24, IEEE, pp. 283–290.
[36] Anselin, L., 1995, "Local Indicators of Spatial Association–LISA," Geograph. Anal., **27**(2), pp. 93–115.